EUROPEAN ORGANIZATION FOR NUCLEAR RESEARCH

CERN-PH-EP/2005-005
28 February 2005

Measurement of the $K_L \to e^+ e^- e^+ e^-$ Decay Rate

A. Lai, D. Marras
Dipartimento di Fisica dell'Università e Sezione dell'INFN di Cagliari, I-09100 Cagliari, Italy.

A. Bevan, R.S. Dosanjh, T.J. Gershon, B. Hay[1)], G.E. Kalmus, C. Lazzeroni, D.J. Munday, M.D. Needham[2)], E. Olaiya, M.A. Parker, T.O. White, S.A. Wotton
Cavendish Laboratory, University of Cambridge, Cambridge, CB3 0HE, U.K.[3)]

G. Barr, G. Bocquet, A. Ceccucci, T. Cuhadar, D. Cundy, G. D'Agostini, N. Doble, V. Falaleev, L. Gatignon, A. Gonidec, B. Gorini, G. Govi, P. Grafström, W. Kubischta, A. Lacourt, A. Norton, S. Palestini, B. Panzer-Steindel, G. Tatishvili[4)], H. Taureg, M. Velasco, H. Wahl[5)]
CERN, CH-1211 Genève 23, Switzerland.

C. Cheshkov, P. Hristov, V. Kekelidze, D. Madigojine, N. Molokanova, Yu. Potrebenikov, A. Zinchenko
Joint Institute for Nuclear Research, Dubna, Russian Federation.

I. Knowles, V. Martin, R. Sacco, A. Walker
Department of Physics and Astronomy, University of Edinburgh, JCMB King's Buildings, Mayfield Road, Edinburgh, EH9 3JZ, U.K.

M. Contalbrigo, P. Dalpiaz, J. Duclos, P.L. Frabetti, A. Gianoli, M. Martini, F. Petrucci, M. Savrié
Dipartimento di Fisica dell'Università e Sezione dell'INFN di Ferrara, I-44100 Ferrara, Italy.

A. Bizzeti[6)], M. Calvetti, G. Collazuol[7)], G. Graziani, E. Iacopini, M. Lenti, G. Ruggiero
Dipartimento di Fisica dell'Università e Sezione dell'INFN di Firenze, I-50125 Firenze, Italy.

[1)] Present address: EP Division, CERN, 1211 Genève 23, Switzerland.
[2)] Present address: NIKHEF, PO Box 41882, 1009 DB Amsterdam, The Netherlands.
[3)] Funded by the U.K. Particle Physics and Astronomy Research Council.
[4)] On leave from Joint Institute for Nuclear Research, Dubna, 141980, Russian Federation
[5)] Also at Dipartimento di Fisica dell'Università e Sezione dell'INFN di Ferrara, I-44100 Ferrara, Italy
[6)] Dipartimento di Fisica dell'Università di Modena e Reggio Emilia, via G. Campi 213/A I-41100 Modena, Italy
[7)] Present address: Scuola Normale Superiore e Sezione INFN di Pisa, I-56100 Pisa, Italy.

H.G. Becker, M. Eppard, H. Fox[8], K. Eppard, A. Kalter, K. Kleinknecht, U. Koch, L. Köpke, P. Lopes da Silva, P. Marouelli, I. Melzer-Pellmann, A. Peters, B. Renk, S.A. Schmidt, V. Schönharting, Y. Schué, R. Wanke, A. Winhart, M. Wittgen
Institut für Physik, Universität Mainz, D-55099 Mainz, Germany[9].

J.C. Chollet, L. Fayard, L. Iconomidou-Fayard, J. Ocariz, G. Unal, I. Wingerter-Seez
Laboratoire de l'Accélératur Linéaire, IN2P3-CNRS, Université de Paris-Sud, 91406 Orsay, France[10].

G. Anzivino, P. Cenci, E. Imbergamo, G. Lamanna[11], P. Lubrano, A. Mestvirishvili, A. Nappi, M. Pepe, M. Piccini
Dipartimento di Fisica dell'Università e Sezione dell'INFN di Perugia, I-06100 Perugia, Italy.

R. Casali, C. Cerri, M. Cirilli[12] , F. Costantini, R. Fantechi, L. Fiorini, S. Giudici, I. Mannelli, G. Pierazzini, M. Sozzi
Dipartimento di Fisica, Scuola Normale Superiore e Sezione INFN di Pisa, I-56100 Pisa, Italy.

J.B. Cheze, J. Cogan[13], M. De Beer, P. Debu, A. Formica, R. Granier de Cassagnac[14], E. Mazzucato, B. Peyaud, R. Turlay, B. Vallage
DSM/DAPNIA - CEA Saclay, F-91191 Gif-sur-Yvette, France.

M. Holder, A. Maier, M. Ziolkowski
Fachbereich Physik, Universität Siegen, D-57068 Siegen, Germany[15].

R. Arcidiacono, C. Biino, N. Cartiglia, F. Marchetto, E. Menichetti, N. Pastrone
Dipartimento di Fisica Sperimentale dell'Università e Sezione dell'INFN di Torino, I-10125 Torino, Italy.

J. Nassalski, E. Rondio, M. Szleper, W. Wislicki, S. Wronka
Soltan Institute for Nuclear Studies, Laboratory for High Energy Physics, PL-00-681 Warsaw, Poland[16].

H. Dibon, G. Fischer, M. Jeitler, M. Markytan, I. Mikulec, G. Neuhofer, M. Pernicka, A. Taurok, L. Widhalm
Österreichische Akademie der Wissenschaften, Institut für Hochenergiephysik, A-1050 Wien, Austria[17].

---

[8] Present address: Physikalisches Institut, Universität Freiburg, D-79104 Freiburg, Germany.

[9] Funded by the German Federal Minister for Research and Technology (BMBF) under contract 7MZ18P(4)-TP2.

[10] Funded by Institut National de Physique des Particules et de Physique Nucléaire (IN2P3), France

[11] Present address: Dipartimento di Fisica dell' Università di Pisa e Sezione INFN di Pisa.

[12] Present address: CERN, CH-1211 Genève 23, Switzerland.

[13] Present address: Centre de Physique des Particules de Marseille, Université de la Méditerranée, IN2P3-CNRS, F-13288 Marseille, France.

[14] Present address: Laboratoire Leprince-Ringuet, Ecole Polytechnique, IN2P3-CNRS, F-91128 Palaiseau, France.

[15] Funded by the German Federal Minister for Research and Technology (BMBF) under contract 056SI74.

[16] Supported by the Committee for Scientific Research grant 2P03B07615 and using computing resources of the Interdisciplinary Center for Mathematical and Computational Modelling of the University of Warsaw.

Submitted for publication in Physics Letters B.

[17] Funded by the Austrian Ministery for Traffic and Research under the contract GZ 616.360/2-IV GZ 616.363/2-VIII, and by the Fonds für Wissenschaft und Forschung FWF Nr. P08929-PHY

Abstract

The decay rate of the long-lived neutral K meson into the $e^+e^-e^+e^-$ final state has been measured with the NA48 detector at the CERN SPS. Using data collected in 1998 and 1999, a total of 200 events has been observed with negligible background. This observation corresponds to a branching ratio of $\mathrm{Br}(\mathrm{K_L} \to \mathrm{e^+\,e^-\,e^+\,e^-}) = (3.30 \pm 0.24_{\mathrm{stat}} \pm 0.23_{\mathrm{sys}} \pm 0.10_{\mathrm{norm}}) \times 10^{-8}$.

1 Introduction

The $K_{\mathrm{L}} \to e^+\,e^-\,e^+\,e^-$ decay is expected to proceed mainly via the intermediate state $K_{\mathrm{L}} \to \gamma^*\gamma^*$ [1, 2] and thus depends on the structure of the $K_{\mathrm{L}} \to \gamma^*\gamma^*$ vertex. Phenomenological models include vector meson dominance of the photon propagator [3], QCD inspired models [4], intermediate pseudo-scalar and vector mesons [5] and models based on chiral perturbation theory [6]. The probability for both virtual photons to convert into e^+e^- pairs is calculated to be in the range $(5.89-6.50)\times10^{-5}$ [2, 7]. The chiral model prediction of [7] corresponds to $\mathrm{Br}(\mathrm{K_L} \to \mathrm{e^+\,e^-\,e^+\,e^-}) = 3.85\times10^{-8}$, including the effect of a form factor, which increases the width by 4%. The interference term due to the identity of particles has been calculated to change the branching ratio by only 0.5%.

The decay was first observed by the CERN NA31 experiment [8] based on 2 observed events and has been confirmed by later measurements [9]. Here we report the result obtained from the 1998 and 1999 data taking periods by the NA48 experiment at the CERN SPS.

2 Experimental Setup and Data Taking

The NA48 experiment is designed specifically to measure the direct CP violation parameter $\mathrm{Re}(\epsilon'/\epsilon)$ using simultaneous beams of K_{L} and K_{S}. To produce the K_{L} beam, 450 GeV/c protons are extracted from the accelerator during 2.4 s every 14.4 s and 1.1×10^{12} of these are delivered to a beryllium target. Using dipole magnets to sweep away charged particles and collimators to define a narrow beam, a neutral beam of 2×10^7 K_{L} per burst and divergence ±0.15 mrad enters the decay region. The fiducial volume begins 126 m downstream of the target and is contained in an evacuated cylindrical steel vessel 89 m long and 2.4 m in maximum diameter. The vessel is terminated at the downstream end by a Kevlar-fiber composite window of a thickness corresponding to 3×10^{-3} radiation lenght and is followed immediately by the main NA48 detector. The sub-detectors which are used in the $K_{\mathrm{L}} \to e^+\,e^-\,e^+\,e^-$ analysis are described below.

A magnetic spectrometer consisting of a dipole magnet is preceded and followed by two sets of drift chambers. The drift chambers are each comprised of eight planes of sense wires, two horizontal, two vertical and two along each of the 45° directions. Only the vertical and horizontal planes are instrumented in the third chamber. The volume between the chambers is filled with helium at atmospheric pressure. The momentum resolution is $\Delta p/p = 0.65\%$ at 45 GeV/c.

Two segmented plastic scintillator hodoscope planes are placed after the helium tank and provide signals for the trigger.

A liquid krypton filled calorimeter (LKr) is used for measuring the energy, position and time of electromagnetic showers. Space and time resolutions of better than 1.3 mm and 300 ps, respectively, have been achieved for energies above 20 GeV. The energy resolution was determined to be $\frac{\sigma(E)}{E} = \frac{0.032}{\sqrt{E}} \oplus \frac{0.090}{E} \oplus 0.0042$, with E measured in GeV.

A hadron calorimeter composed of 48 steel plates, each 24 mm thick, interleaved with scintillator is used in trigger formation and for particle identification.

A detailed description of the detector can be found in [10].

The data used in this analysis were recorded in the 1998-1999 data taking period. Candidate events were selected by a two-stage trigger. At the first level, a trigger requiring adjacent hits in the hodoscope is put in coincidence with a total energy condition ($\geq$ 35 GeV), defined by adding the energy deposited in the hadronic calorimeter with that seen by the trigger in the LKr calorimeter. The second level trigger uses information from the drift chambers to reconstruct tracks and invariant masses. For the 4-track part of the trigger, the number of clustered hits in each of the first, second, and fourth drift chamber had to be between 3 and 7. All possible 2-track vertices were calculated online. At least two vertices within 6 m of each other in the axial direction had to be found. In order to determine the efficiency of the 4-track trigger, downscaled events that passed a trigger based just on the total energy condition were recorded (the downscaling factor changed from 100 to 60 depending on the data taking period). More details on the 4-track trigger can be found in [12].

3 Data Analysis

The decay vertex of candidate events was reconstructed from the 4-track barycenter position in the transverse direction, calculated as a function of the vertex longitudinal position; each track is weighted by its momentum to take into account the multiple scattering effect. The 4-track vertex longitudinal position was calculated by minimizing the sum of the squared transverse distance of each track from the transverse vertex position; the closest distance of approach of the 4-track vertex is defined as the square root of this sum at its minimum.

Events were preselected by requiring two positive and two negative tracks; each couple of tracks must form a 2-track vertex with distance of closest approach smaller than 10 cm and an axial position of the vertex less than 210 m downstream of the target; each track must be compatible in time with any other within 8 ns.

The tracks extrapolated at the LKr were required to be in a fiducial area given by an octagon about 5 cm smaller than the outside perimeter of the calorimeter and an inner radius of 15 cm; the distance to any dead calorimeter cell (about 80 out of 13500) had to exceed 2 cm. The separation between each track extrapolated at LKr entry face was required to be greater than 5 cm. The momentum of each track, measured by the magnetic spectrometer, was required to exceed 2 GeV, well above the detector noise of 100 MeV per cluster in the LKr.

Electron candidates were identified by requiring that cluster centers in the LKr be within 1.5 cm of the extrapolation of each track (the rms width of electromagnetic showers in LKr is 2.2 cm). To reject pion showers, the ratio of cluster energy to track momentum E/p was required to be greater than 0.9. Track-associated clusters with $E/p < 0.8$ were classified as pions.

The fiducial volume was defined by the axial position of the vertex being between 127.5 m and 210 m downstream of the target. Within this volume, 4-track vertices were determined with a typical longitudinal resolution of 0.5 m, as estimated by the Monte Carlo simulation. The total energy had to be within 50 GeV and 200 GeV.

3.1 Selection of $K_{\rm L} \to e^+\,e^-\,e^+\,e^-$ Candidates and Background Rejection

Candidate events for the decay $K_{\rm L} \to e^+\,e^-\,e^+\,e^-$ with all tracks identified as electrons were selected. The following four classes of background sources were relevant:

- Events with two decays $K_{\rm L} \to \pi e \nu$ occurring at the same time and for which the pions were misidentified as electrons. Being due to two coincident kaon decays the invariant mass of the system could be around and above the nominal $K_{\rm L}$ mass. These events were largely rejected by requiring a good vertex quality: the 4-track vertex closest distance of approach (defined above) had to be smaller than 5 cm. Because of missing transverse momentum in this and most other background decays, we required the square of the transverse momentum p_t^2 of the reconstructed kaon with respect to the line joining the decay vertex and the $K_{\rm L}$ target to be less than 0.0005 (GeV/c)^2. We chose not to cut harder in order to include most signal events with final state radiation. The position of the cut is indicated in Fig. 1. The Monte Carlo simulation indicates that 8.3% of the signal events were lost by the requirement on p_t^2. In addition, as already mentioned in the preselection, it was required that each track be compatible in time with any other within 8 ns. A study of sidebands in this time distribution shows that the background from this source was negligible.
- Events $K_{\rm L} \to \pi^0\pi^0, \pi^0\pi^0\pi^0$, where the π^0s undergo single or double Dalitz decays or photons convert in the material of the detector, so that 2 positive and 2 negative electrons are detected. Due to the missing photons, the invariant mass of the $e^+e^-e^+e^-$ system is below the nominal $K_{\rm L}$ mass.
- Events $K_{\rm L} \to \gamma\gamma$ and $K_{\rm L} \to e^+e^-\gamma$, with conversion of the photons in the material upstream of the spectrometer also yield invariant masses around the nominal $K_{\rm L}$ mass. The conversion probability in the material of the NA48 detector is of similar magnitude as that for internal photon conversion to a e^+e^- pair. Each pair of oppositely charged tracks was therefore required to be separated by more than 2 cm in the first drift chamber. According to the Monte Carlo simulation, there was no remaining background with converted photons.
- Events $K_{\rm L} \to \pi^+\pi^-e^+e^-$ [11, 12], with the pions misidentified as electrons. Due to the misidentification probability of 0.5% [13] this background was found to be negligible.

The invariant $e^+e^-e^+e^-$ mass distribution resulting from this selection is shown in Fig. 2. Note the slightly asymmetric shape of the $K_{\rm L}$ mass peak, which is due to photons radiated off the electrons in the final state.

Finally, a mass window of 475 MeV/c^2 $< m(e^+e^-e^+e^-) <$ 515 MeV/c^2 was set to define the final sample. In total, 200 candidate events were selected, 62 from the 1998 data period and 138 from the 1999 one.

The Monte Carlo simulation of the background shows that the contribution from $K_{\rm L} \to \pi^+\pi^-\pi^0_{\rm Dalitz}$, $K_{\rm L} \to \pi^0\pi^0_{\rm Dalitz}\pi^0_{\rm Dalitz}$ and $K_{\rm L} \to \pi^0_{\rm Dalitz}\pi^0_{\rm Dalitz}$ decays in the signal region was negligible (less than 0.1% at 90% C.L.). As a cross-check in the data, we defined a control region $0.0010 < p_t^2 < 0.0020$ (GeV/c)^2 and 475 MeV/c^2 $< m(e^+e^-e^+e^-) <$ 515 MeV/c^2, where 0 events were found: assuming an upper limit of 2.30 events (90% C.L.), the extrapolation from the high p_t control region to the low p_t signal region was made using a $0.2 < m(e^+e^-e^+e^-) < 0.4$ GeV/c^2 interval for normalization; the upper limit on the background in the signal region turned out to be 0.8%. Varying the control and normalization region limits we obtained an upper limit on the background of 1% that was used as the systematic uncertainty for the background.

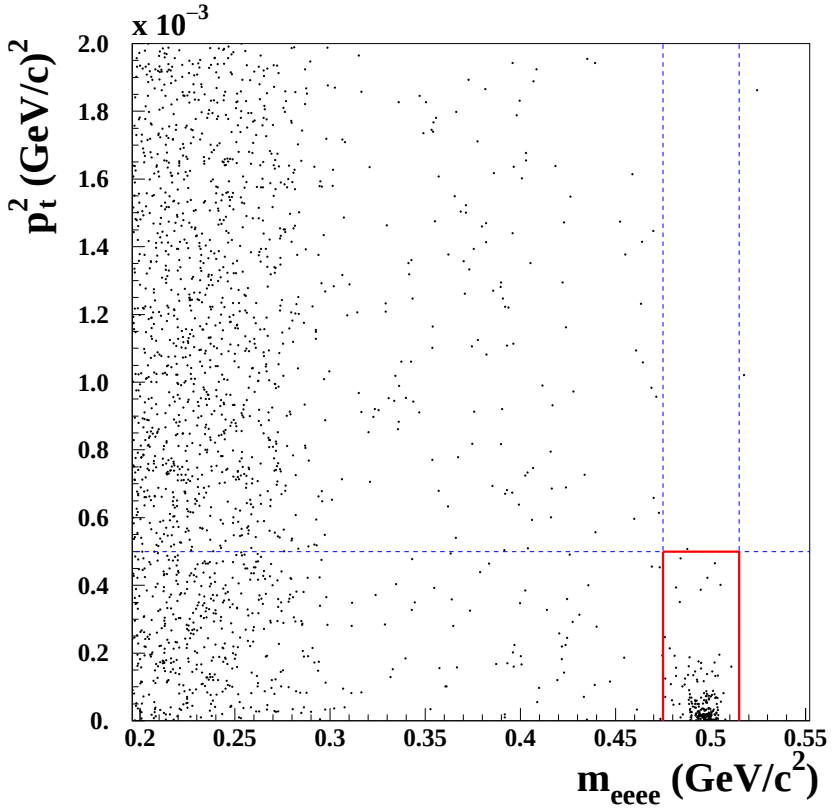

Figure 1: *Correlation of $e^+e^-e^+e^-$ invariant mass with the squared transverse momentum p_t^2 of the reconstructed kaon. The box is the signal region*

3.2 Normalization

The four-track decay $K_{\rm L} \to \pi^+\pi^-\pi^0_{\rm Dalitz}$, with $\pi^0_{\rm Dalitz} \to e^+e^-\gamma$, was used for normalization. Events that passed the same trigger as the signal events were selected. Since both the signal and the normalization modes consist of 4-track events, uncertainties due to tracking tend to cancel in the ratio of acceptances. Selection criteria similar to those used in the signal mode were applied. The distance between each electron/positron and each pion had to be greater than 10 cm on the tracks extrapolated to the LKr, due to the size of the pion hadronic shower.

In addition, at least one extra cluster in the calorimeter with energy larger than 2 GeV, separated by more than 15 cm from each extrapolated track was required, with a time compatible within 3 ns with the average track time.

The invariant mass of the $e^+e^-\gamma$ system was required to be in the range of 120 – 140 MeV/c^2 and the invariant mass of the $\pi^+\pi^-\pi^0_{\rm Dalitz}$ system had to be in the range of 475 – 515 MeV/c^2. Monte Carlo studies showed that background from $K_{\rm L} \to \pi^+\pi^-\pi^0$ with one of the external photons converting in the material of the detector was completely eliminated by the requirement on the minimum distance of the electron tracks in the first drift chamber being larger than 2 cm. All other backgrounds have been estimated to be negligible. After applying all selection criteria, a total of 2.988×10^6 $K_{\rm L} \to \pi^+\pi^-\pi^0_{\rm Dalitz}$ decays were found (0.822×10^6 in the 1998 data sample and 2.166×10^6 in the 1999 one).

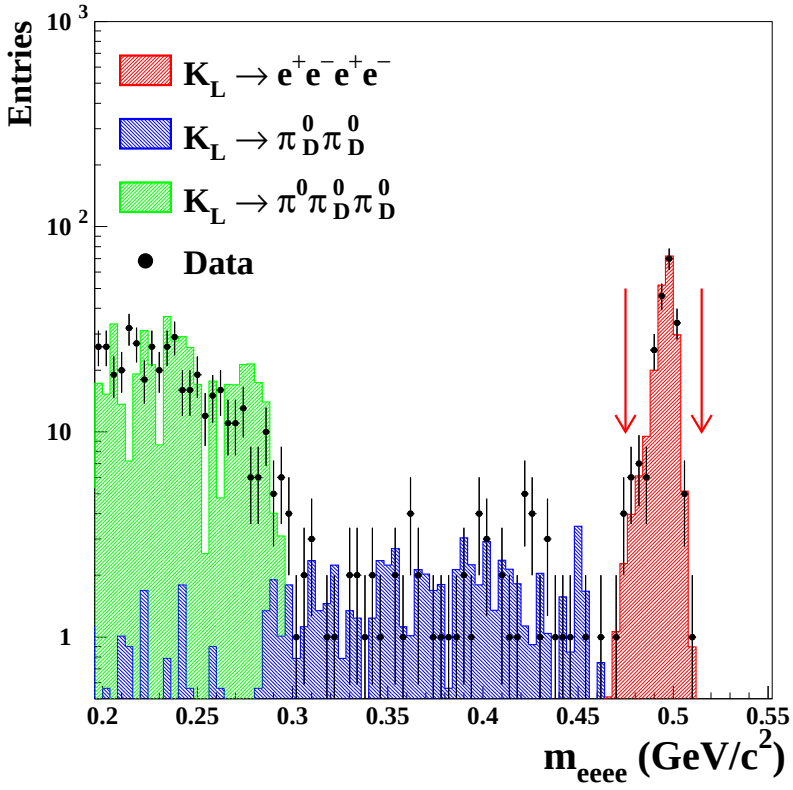

Figure 2: *Invariant mass of the $e^+e^-e^+e^-$ system. The data are shown as dots with error bars, the Monte Carlo prediction for the signal and backgrounds, normalized to the data, is shown as histogram. The position of the mass cut is also indicated.*

3.3 Acceptance Determination and Systematic Uncertainty

For the simulation of the $K_{\rm L} \to e^+\,e^-\,e^+\,e^-$ acceptance, the matrix element was taken from Ref. [2], taking into account the direct and exchange graph but neglecting the interference term; the decay form factor was assumed to be a constant. The distribution of the angle spanned by the decay planes of the two e^+e^- pairs corresponds to a $K_{\rm L}$ which is assumed to be entirely CP= -1. The PHOTOS [15] package was used to simulate final state radiation both for the signal and normalization channels. The simulation is based on the GEANT 3.21 package [16]. It includes a detailed description of the spectrometer and a GEANT-based shower library for the calorimeter response.

The 4-track trigger efficiency for the normalization channel was studied using a large sample of fully reconstructed $K_{\rm L} \to \pi^+\pi^-\pi^0_{\rm Dalitz}$ events that was collected with the downscaled control trigger. The efficiency of the 4-track trigger algorithm relative to the first level trigger was measured to be $(89.0 \pm 0.2)\%$ in 1999 and $(69.4 \pm 0.4)\%$ in 1998 [1)].

The difference between signal and normalization trigger efficiency should cancel when computing the decay rate. We cross-checked this assumption by comparing the 4-track trigger efficiency as a function of 4-track total energy (instead of the kaon energy) with the signal spectrum. We also used a partially biased not downscaled trigger based only on LKr information to cross-check directly the signal trigger efficiency, obtaining

[1)] The 4-track trigger used 200 MHz processors in 1998 and was upgraded with 300 MHz ones in 1999, allowing complex events to be treated more efficiently.

results in agreement with the previous method. We assigned a systematic uncertainty of 2% to the 4-track trigger efficiency.

In order to be insensitive to the real kaon energy spectrum, the acceptance correction was applied to the data in bins of kaon energy (5 GeV wide) and the corresponding average $K_{\rm L} \to e^+ e^- e^+ e^- / K_{\rm L} \to \pi^+\pi^-\pi^0_{\rm Dalitz}$ acceptance ratio was evaluated to be 2.89. The average acceptance for $K_{\rm L} \to e^+ e^- e^+ e^-$ was 5.67% and 2.03% for $K_{\rm L} \to \pi^+\pi^-\pi^0_{\rm Dalitz}$ decays, for events generated in the range 50 GeV $< E_{K_{\rm L}} <$ 200 GeV and 127.5 m $< z_{vertex} <$ 210 m. The 3% difference between the binned acceptance ratio and the ratio of the average acceptances was used as systematic uncertainty on the acceptance correction.

The inclusion of radiative corrections in the Monte Carlo generator decreased the acceptance by 8.8% for the signal and 3.4% for the normalization. The 5.6% net effect on the branching ratio was used as systematic uncertainty on radiative corrections.

The E/p cut, either for the signal or for the normalization channel, is not well simulated by the Monte Carlo and its efficiency was calculated using the data. Pions were tagged by a sample of $K_{\rm L} \to \pi^+\pi^-\pi^0_{\rm Dalitz}$ where 3 out of 4 tracks are positively identified, while for electrons, a sample of $K_{\rm L} \to \pi^0\pi^0_{\rm Dalitz}\pi^0_{\rm Dalitz}$ was also used. The requirement of 3 identified tracks in these samples could slightly bias the E/p cut efficiency for the fourth track due to the energy sharing among clusters; in order to control this effect, a measurement of the E/p cut efficiency was also performed on samples of $K_{\rm L} \to \pi^+\pi^-\pi^0_{\rm Dalitz}$ or $K_{\rm L} \to \pi^0\pi^0_{\rm Dalitz}\pi^0_{\rm Dalitz}$ decays without any request on the identification of the tracks: these samples were not completely background free and, in case of very low E/p for more than one track, were also affected by a lower calorimetric trigger efficiency; nevertheless they gave a E/p cut efficiency in agreement with the first method within 2%. The different electron momentum spectrum in the signal and in the control sample and the momentum dependence of the E/p cut efficiency were taken into account. The correction induced by the E/p cut decreases the branching ratio by a factor of 0.944 ± 0.020 where the error is systematic.

In the following table the different contributions to the systematic uncertainty are listed.

Table 1: Systematic uncertainty contributions to $\mathrm{Br(K_L \to e^+ e^- e^+ e^-)}$

Source	
Trigger efficiency	$\pm$2.0%
Background estimation	$\pm$1.0%
E/p cut efficiency	$\pm$2.0%
Detector acceptance	$\pm$3.0%
Radiative corrections	$\pm$5.6%
Total	$\pm$7.0%

4 Results and Discussion

We used for the normalization channel the value [14]:

$$BR(K_L \to \pi^+\pi^-\pi^0_D) = BR(K_L \to \pi^+\pi^-\pi^0) \times BR(\pi^0 \to e^+e^-\gamma) =$$

$$= (12.59 \pm 0.19)\% \times (1.198 \pm 0.032)\% = (15.08 \pm 0.46) \times 10^{-4}$$

From the numbers given above for the entire 1998 and 1999 data sample, a branching ratio of

$$\mathrm{Br(K_L \to e^+ e^- e^+ e^-)} = (3.30 \pm 0.24_{\rm stat} \pm 0.23_{\rm syst} \pm 0.10_{\rm norm}) \times 10^{-8}$$

was obtained, where the statistical and systematic uncertainties as well as the uncertainty in the $K_{\rm L} \to \pi^+\pi^-\pi^0_{\rm Dalitz}$ branching ratio are given separately.

A study of the stability of the branching ratio determination was made as a function of the cuts applied: the variation is within the estimated systematic uncertainty. Both the 1998 and 1999 data samples gave consistent results within one standard deviation.

In addition, $K_{\rm L} \to \pi^0\pi^0_{\rm Dalitz}\pi^0_{\rm Dalitz}$ has been used as normalization channel obtaining a result in agreement with the above one.

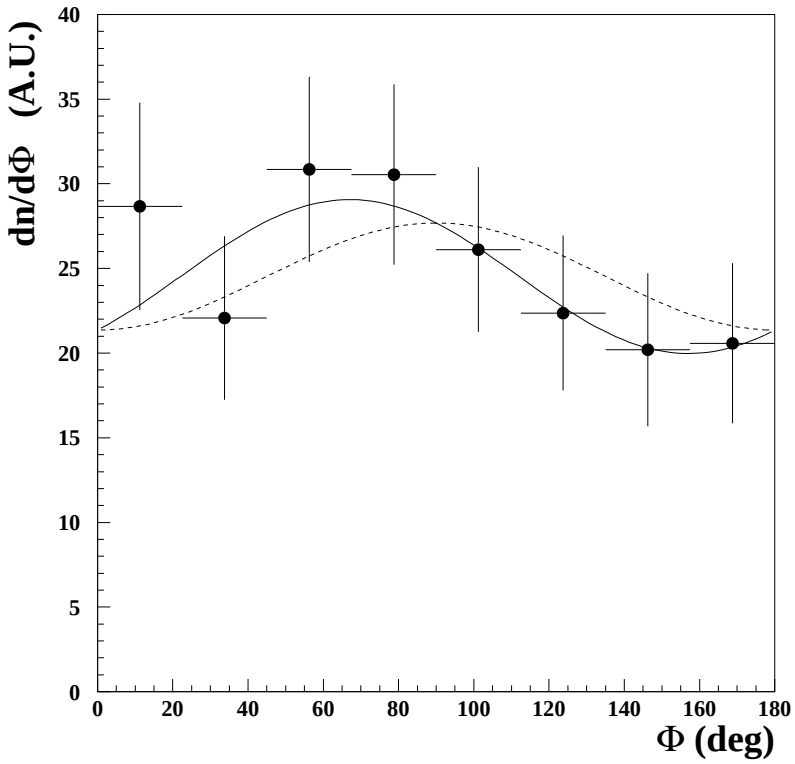

Figure 3: *The acceptance corrected ϕ distribution of the data (dots with error bars) in arbitrary units. The result of the fit with β_{CP} and γ_{CP} as free parameters is shown as a solid line; the fit with $\gamma_{CP} \equiv 0$ is also shown (dashed line).*

As shown in[9], the angle ϕ between the two planes spanned by each e^+e^- pair can be used to determine the CP value of the $K_{\rm L}$ meson. In the limit of no direct CP violation, the angular distribution in ϕ is given by [17, 18]

$$\frac{dn}{d\phi} \propto 1 + \beta_{CP}\,\cos 2\phi + \gamma_{CP}\,\sin 2\phi,$$

$$\text{with} \qquad \beta_{CP} = \frac{1-|\epsilon\, r|^2}{1+|\epsilon\, r|^2}\, B, \qquad \gamma_{CP} = \frac{2\,\mathrm{Re}(\epsilon\, r)}{1+|\epsilon\, r|^2}\, C,$$

and the parameter ϵ of indirect CP violation and the ratio r of the amplitudes for K_1 and K_2 decaying into the $e^+e^-e^+e^-$ final state. In the limit of no indirect CP violation, the term in $\sin 2\phi$ vanishes and the classical formula by Kroll and Wada is obtained, with

the constant $B = \pm 0.20$ for CP $= \pm 1$ coming from integration over phase space. At the moment no calculation exists for C.

For the measurement of the angle ϕ, the ambiguity in the e^+e^- pairing was resolved by choosing the combination that minimized the product of invariant masses of the two pairs. Monte Carlo studies showed that in 98% of the cases we obtain the correct combination by this method. The remaining wrong pairings are uniformly distributed in ϕ. The acceptance corrected ϕ distribution is shown in Fig. 3. By fitting this distribution we measured $\beta_{CP} = -0.13 \pm 0.10_{stat} \pm 0.03_{sys}$ and $\gamma_{CP} = 0.13 \pm 0.10_{stat} \pm 0.03_{sys}$. Clearly, the obtained precision on the parameters β_{CP} and γ_{CP} is limited by the event statistics. The main sources for the systematic uncertainties are the ϕ dependence of the detector acceptance and the effect of wrong pairings. By imposing $\gamma_{CP} = 0$, the fitted value of β_{CP} is $-0.13 \pm 0.10_{stat}$. Our result is consistent with the hypothesis of a CP $= -1$ amplitude as expected from a K_L decay.

Acknowledgements

It is a pleasure to thank the technical staff of the participating laboratories, universities and affiliated computing centers for their efforts in the construction of the NA48 apparatus, in operation of the experiment, and in the processing of the data.

References

[1] Z.E.S. Uy, Phys. Rev. **D43** (1991) 802 and Phys. Rev. **D43** (1991) 1572;
T. Miyasaki, Nuovo Cimento **5** (1972) 125.
[2] T. Miyazaki and E. Taksugi, Phys. Rev. **D8** (1973) 2051.
[3] J.J. Sakurai, Phys. Rev. **156** (1967) 1508;
M. Moshe and P. Singer, Phys. Rev. **D6** (1972) 1379.
[4] M.A. Shifman *et al.*, Nucl. Phys. **B120** (1977) 316.
[5] L. Bergström *et al.*, Phys. Lett. **B131** (1983) 229.
[6] G. D'Ambrosio and J. Portoles, J. Nucl. Phys. **B492** (1997) 417;
J.L. Goity and L. Zhang, Phys. Lett. **B398** (1997) 3874.
[7] L. Zhang and J.L. Goity, Phys. Rev. **D57** (1998) 7031.
[8] G.D. Barr *et al.*, Phys. Lett. **B259** (1991) 389.
[9] M.R. Vagins *et al.*, Phys. Rev. Lett. **71** (1993) 35;
T. Akagi *et al.*, Phys. Rev. **D47** (1993) R2644;
P. Gu *et al.*, Phys. Lett. **72** (1994) 3000;
G.D. Barr *et al.*, Z. Phys. **C65** (1995) 361;
T. Akagi *et al.*, Phys. Rev. **D51** (1995) 2061);
A. Alavi-Harati *et al.*, Phys. Rev. Lett. **86** (2001) 5425.
[10] A. Lai *et al.*, Eur. Phys. J **C22** (2001) 231.
[11] A. Alavi-Harati *et al.*, Phys. Rev. Lett. **84** (2000) 408.
[12] A. Lai *et al.*, Eur. Phys. J **C30** (2003) 33.
[13] A. Lai *et al.*, Phys. Lett. **B602** (2004) 41.
[14] Particle Data Group, Phys. Lett. **592** (2004) 1.
[15] E. Barbario, B. van Eijk, and Z. Was, Comput. Phys. Commun. **66**, (1991) 115.
[16] GEANT Detector Description and Simulation Tool, CERN Program Library Long Write-up W5013 (1994).
[17] N.M. Kroll and W. Wada, Phys. Rev. **98** (1955) 1355.
[18] P. Gu *et al.*, Phys. Rev. Lett. **72** (1994) 3000.